Second harmonic generation from nanocrystals under linearly and circularly polarized excitations

Chia-Lung Hsieh,[1,2*] Ye Pu,[1] Rachel Grange,[1] and Demetri Psaltis[1]

[1]*School of Engineering, EPFL, Station 17, 1015 Lausanne, Switzerland*
[2]*Department of Electrical Engineering, California Institute of Technology, 1200 East California Boulevard, MC 136-93, Pasadena, California 91125, USA*
**chia-lung.hsieh@epfl.ch*

Abstract: We study second harmonic generation (SHG) from non-centrosymmetric nanocrystals under linearly polarized (LP) and circularly polarized (CP) excitations. Theoretical models are developed for SHG from nanocrystals under both plane-wave and focused excitations. We find that the focused excitation reduces the polarization dependency of the SHG signal. We show that the SHG response under CP excitation is generally inferior to the average of LP excitations over all orientations. We verify the theory by measuring the SHG polar responses from $BaTiO_3$ nanocrystals with a scanning confocal microscope. The experimental data agrees well with the theory.

OCIS codes: (160.4236) Nanomaterials; (160.4330) Nonlinear optical materials; (180.4315) Nonlinear microscopy; (260.5430) Polarization; (320.7110) Ultrafast nonlinear optics.

References and links

1. I. Freund, M. Deutsch, and A. Sprecher, "Connective tissue polarity. Optical second-harmonic microscopy, crossed-beam summation, and small-angle scattering in rat-tail tendon," Biophys. J. **50**(4), 693–712 (1986).
2. S. W. Chu, I. H. Chen, T. M. Liu, P. C. Chen, C. K. Sun, and B. L. Lin, "Multimodal nonlinear spectral microscopy based on a femtosecond Cr:forsterite laser," Opt. Lett. **26**(23), 1909–1911 (2001).
3. P. J. Campagnola, A. C. Millard, M. Terasaki, P. E. Hoppe, C. J. Malone, and W. A. Mohler, "Three-dimensional high-resolution second-harmonic generation imaging of endogenous structural proteins in biological tissues," Biophys. J. **82**(1), 493–508 (2002).
4. A. Zoumi, A. Yeh, and B. J. Tromberg, "Imaging cells and extracellular matrix in vivo by using second-harmonic generation and two-photon excited fluorescence," Proc. Natl. Acad. Sci. U.S.A. **99**(17), 11014–11019 (2002).
5. P. J. Campagnola, and L. M. Loew, "Second-harmonic imaging microscopy for visualizing biomolecular arrays in cells, tissues and organisms," Nat. Biotechnol. **21**(11), 1356–1360 (2003).
6. K. Konig, and I. Riemann, "High-resolution multiphoton tomography of human skin with subcellular spatial resolution and picosecond time resolution," J. Biomed. Opt. **8**(3), 432–439 (2003).
7. W. R. Zipfel, R. M. Williams, R. Christie, A. Y. Nikitin, B. T. Hyman, and W. W. Webb, "Live tissue intrinsic emission microscopy using multiphoton-excited native fluorescence and second harmonic generation," Proc. Natl. Acad. Sci. U.S.A. **100**(12), 7075–7080 (2003).
8. P. Stoller, K. M. Reiser, P. M. Celliers, and A. M. Rubenchik, "Polarization-modulated second harmonic generation in collagen," Biophys. J. **82**(6), 3330–3342 (2002).
9. S. W. Chu, S. Y. Chen, G. W. Chern, T. H. Tsai, Y. C. Chen, B. L. Lin, and C. K. Sun, "Studies of chi(2)/chi(3) tensors in submicron-scaled bio-tissues by polarization harmonics optical microscopy," Biophys. J. **86**(6), 3914–3922 (2004).
10. R. M. Williams, W. R. Zipfel, and W. W. Webb, "Interpreting second-harmonic generation images of collagen I fibrils," Biophys. J. **88**(2), 1377–1386 (2005).
11. S. V. Plotnikov, A. C. Millard, P. J. Campagnola, and W. A. Mohler, "Characterization of the myosin-based source for second-harmonic generation from muscle sarcomeres," Biophys. J. **90**(2), 693–703 (2006).
12. J. C. Johnson, H. Q. Yan, R. D. Schaller, P. B. Petersen, P. D. Yang, and R. J. Saykally, "Near-field imaging of nonlinear optical mixing in single zinc oxide nanowires," Nano Lett. **2**(4), 279–283 (2002).
13. S. Brasselet, V. Le Floc'h, F. Treussart, J. F. Roch, J. Zyss, E. Botzung-Appert, and A. Ibanez, "In situ diagnostics of the crystalline nature of single organic nanocrystals by nonlinear microscopy," Phys. Rev. Lett. **92**(20), 4 (2004).

#126083 - $15.00 USD Received 26 Mar 2010; revised 10 May 2010; accepted 13 May 2010; published 21 May 2010

14. E. Delahaye, N. Tancrez, T. Yi, I. Ledoux, J. Zyss, S. Brasselet, and R. Clement, "Second harmonic generation from individual hybrid MnPS3-based nanoparticles investigated by nonlinear microscopy," Chem, Phys. Lett. **429**, 533–537 (2006).
15. L. L. Xuan, S. Brasselet, F. Treussart, J. F. Roch, F. Marquier, D. Chauvat, S. Perruchas, C. Tard, and T. Gacoin, "Balanced homodyne detection of second-harmonic generation from isolated subwavelength emitters," Appl. Phys. Lett. **89**(12), 121118 (2006).
16. L. Bonacina, Y. Mugnier, F. Courvoisier, R. Le Dantec, J. Extermann, Y. Lambert, V. Boutou, C. Galez, and J. P. Wolf, "Polar Fe(IO3)(3) nanocrystals as local probes for nonlinear microscopy," Appl. Phys. B **87**(3), 399–403 (2007).
17. Y. Nakayama, P. J. Pauzauskie, A. Radenovic, R. M. Onorato, R. J. Saykally, J. Liphardt, and P. D. Yang, "Tunable nanowire nonlinear optical probe," Nature **447**(7148), 1098–1101 (2007).
18. N. Sandeau, L. Le Xuan, D. Chauvat, C. Zhou, J. F. Roch, and S. Brasselet, "Defocused imaging of second harmonic generation from a single nanocrystal," Opt. Express **15**(24), 16051–16060 (2007).
19. A. V. Kachynski, A. N. Kuzmin, M. Nyk, I. Roy, and P. N. Prasad, "Zinc oxide nanocrystals for nonresonant nonlinear optical microscopy in biology and medicine," J. Phys. Chem. C **112**(29), 10721–10724 (2008).
20. X. L. Le, C. Zhou, A. Slablab, D. Chauvat, C. Tard, S. Perruchas, T. Gacoin, P. Villeval, and J. F. Roch, "Photostable second-harmonic generation from a single KTiOPO4 nanocrystal for nonlinear microscopy," Small **4**(9), 1332–1336 (2008).
21. Y. Pu, M. Centurion, and D. Psaltis, "Harmonic holography: a new holographic principle," Appl. Opt. **47**(4), A103–A110 (2008).
22. J. Extermann, L. Bonacina, E. Cuña, C. Kasparian, Y. Mugnier, T. Feurer, and J. P. Wolf, "Nanodoublers as deep imaging markers for multi-photon microscopy," Opt. Express **17**(17), 15342–15349 (2009).
23. C. L. Hsieh, R. Grange, Y. Pu, and D. Psaltis, "Three-dimensional harmonic holographic microcopy using nanoparticles as probes for cell imaging," Opt. Express **17**(4), 2880–2891 (2009).
24. T. R. Kuo, C. L. Wu, C. T. Hsu, W. Lo, S. J. Chiang, S. J. Lin, C. Y. Dong, and C. C. Chen, "Chemical enhancer induced changes in the mechanisms of transdermal delivery of zinc oxide nanoparticles," Biomaterials **30**(16), 3002–3008 (2009).
25. E. M. Rodríguez, A. Speghini, F. Piccinelli, L. Nodari, M. Bettinelli, D. Jaque, and J. G. Sole, "Multicolour second harmonic generation by strontium barium niobate nanoparticles," J. Phys. D Appl. Phys. **42**(10), 4 (2009).
26. E. V. Rodriguez, C. B. de Araujo, A. M. Brito-Silva, V. I. Ivanenko, and A. A. Lipovskii, "Hyper-Rayleigh scattering from BaTiO3 and PbTiO3 nanocrystals," Chem. Phys. Lett. **467**(4-6), 335–338 (2009).
27. P. Wnuk, L. L. Xuan, A. Slablab, C. Tard, S. Perruchas, T. Gacoin, J. F. Roch, D. Chauvat, and C. Radzewicz, "Coherent nonlinear emission from a single KTP nanoparticle with broadband femtosecond pulses," Opt. Express **17**(6), 4652–4658 (2009).
28. M. Zielinski, D. Oron, D. Chauvat, and J. Zyss, "Second-harmonic generation from a single core/shell quantum dot," Small **5**(24), 2835–2840 (2009).
29. C. L. Hsieh, R. Grange, Y. Pu, and D. Psaltis, "Bioconjugation of barium titanate nanocrystals with immunoglobulin G antibody for second harmonic radiation imaging probes," Biomaterials **31**(8), 2272–2277 (2010).
30. S. J. Lin, C. Y. Hsiao, Y. Sun, W. Lo, W. C. Lin, G. J. Jan, S. H. Jee, and C. Y. Dong, "Monitoring the thermally induced structural transitions of collagen by use of second-harmonic generation microscopy," Opt. Lett. **30**(6), 622–624 (2005).
31. M. Strupler, A. M. Pena, M. Hernest, P. L. Tharaux, J. L. Martin, E. Beaurepaire, and M. C. Schanne-Klein, "Second harmonic imaging and scoring of collagen in fibrotic tissues," Opt. Express **15**(7), 4054–4065 (2007).
32. A. C. Kwan, D. A. Dombeck, and W. W. Webb, "Polarized microtubule arrays in apical dendrites and axons," Proc. Natl. Acad. Sci. U.S.A. **105**(32), 11370–11375 (2008).
33. B. Richards, and E. Wolf, "Electromagnetic diffraction in optical systems. 2. Structure of the image field in an aplanatic system," Proceedings of the Royal Society of London Series a-Mathematical and Physical Sciences **253**, 358–379 (1959).
34. A. A. Asatryan, C. J. R. Sheppard, and C. M. de Sterke, "Vector treatment of second-harmonic generation produced by tightly focused vignetted Gaussian beams," J. Opt. Soc. Am. B **21**(12), 2206–2212 (2004).
35. E. Y. S. Yew, and C. J. R. Sheppard, "Effects of axial field components on second harmonic generation microscopy," Opt. Express **14**(3), 1167–1174 (2006).
36. C. F. Bohren, and D. R. Huffman, "Absorption and Scattering of Light by Small Particles," (Wiley, 1998).
37. R. W. Boyd, *Nonlinear Optics*, Ch. 1 (Academic, New York, 1992), pp. 1–52.
38. J. D. Jackson, *Classical Electrodynamics* (Wiley, New York, 1998), p. 410.
39. C.-K. Chou, W.-L. Chen, P. T. Fwu, S.-J. Lin, H.-S. Lee, and C.-Y. Dong, "Polarization ellipticity compensation in polarization second-harmonic generation microscopy without specimen rotation," J. Biomed. Opt. **13**(1), 014005 (2008).
40. P. Schön, F. Munhoz, A. Gasecka, S. Brustlein, and S. Brasselet, "Polarization distortion effects in polarimetric two-photon microscopy," Opt. Express **16**(25), 20891–20901 (2008).

#126083 - $15.00 USD Received 26 Mar 2010; revised 10 May 2010; accepted 13 May 2010; published 21 May 2010

1. Introduction

Second harmonic generation (SHG) microscopy has been developed as a powerful nonlinear optical imaging tool for examining endogenous structures in biological samples [1–7]. SHG only takes place in a non-centrosymmetric environment, and provides the imaging contrast of specific endogenous biological structures, such as collagen, muscle, and microtubules in a mostly isotropic environment. In biological samples, the molecular structures and orientations determine the nonlinear susceptibility. As a result, the polarization dependent measurement of the SHG signal can be used to study the molecular structures of biological samples [3, 8–11].

While the endogenous SHG signal is attractive for label-free non-invasive imaging, exogenous SHG markers are also desirable due to the flexibility of having the SHG contrast from any target of interest. Recently, efficient SHG from non-centrosymmetric nanomaterials has been reported [12–29]. These nanoparticles emit coherent, non-bleaching and non-blinking SHG signal with a broad flexibility in the choice of excitation wavelength due to the non-resonant SHG process, showing great promises as imaging probes. We therefore refer to these SHG-active nanocrystals as "Second Harmonic Radation IMaging Probes (SHRIMPs)." The coherent SHG signal accommodates interferometric detection of SHRIMPs and therefore offers the benefits of high signal-to-noise ratio and nonscanning three-dimensional imaging [15, 21, 23]. By exploiting the flexibility in the selection of the excitation wavelength, SHRIMPs have also been demonstrated as deep imaging markers [22]. Furthermore, the polarization dependent SHG response of SHRIMPs has been explored at the single-nanocrystal level [12–14, 16, 18, 20, 23, 28], where the orientation of the SHRIMP can be determined in the far field by a polarization measurement.

Despite the merits offered by the polarization sensitive SHG response, it may complicate a spatial distribution measurement of the SHG active targets of different orientations. As a result, circularly polarized (CP) excitation has been frequently adopted as an alternative [30–32]. It is thus important to examine the SHG response under linearly polarized (LP) and CP excitations in SHG nonlinear microscopy. We show in this paper that the SHG response under a CP excitation is generally inferior to the average of the SHG responses under LP excitation over all orientations.

Laser scanning microscopy, such as scanning confocal microscopy, is the most popular SHG microscopy where a high numerical aperture (NA) objective tightly focuses the excitation beam to reach a high local intensity for efficient nonlinear phenomena to take place. The transverse and axial field components generated through tightly focusing the incident laser beam, known as the depolarization effect [33], can significantly modify the overall polarization dependent SHG response [34, 35]. For the detection, the SHG signal is either collected by the same objective in epi-geometry or by another objective in the transmission geometry. A similar depolarization effect should also be considered in the detection for an accurate estimation.

In this paper, we use barium titanate ($BaTiO_3$) nanocrystals to study the SHG response under LP and CP excitations. We consider the depolarization effect introduced by the use of a high NA objective, including a tightly focused beam for the excitation, and also the collection efficiency of both transverse and axial SHG polarization components. We measure the polarization dependent SHG response by a standard scanning confocal microscope. Excellent agreement between the experiments and the theory is observed.

2. Theoretical models of SHG from nanocrystals

2.1 SHG from nanocrystals under a plane-wave excitation

We start our study with a nanocrystal under a uniform LP excitation using $BaTiO_3$ nanocrystals. The crystal structure of the $BaTiO_3$ nanocrystal is tetragonal, which belongs to symmetry class 4 [36]. Due to the crystal symmetry, the SHG response is determined only by the orientation of the c-axis of the nanocrystal, and the rotation of the nanocrystal around the

#126083 - $15.00 USD Received 26 Mar 2010; revised 10 May 2010; accepted 13 May 2010; published 21 May 2010

c-axis has no influence on the SHG response. The orientation of an object in a three-dimensional space can be defined by three Euler angles in an Euler coordinate. To define the orientation of the c-axis in space, the degree of freedom is reduced to two angles which can be described in a spherical coordinate. The orientation of the c-axis of the nanocrystal can be uniquely defined by the angles θ_0 and ϕ_0 in the spherical coordinate as shown in Fig. 1(a). The incident excitation propagates along the Z axis and the excitation polarization angle γ can be rotated in the XY plane by a half wave plate.

Assuming the shape of the nanocrystal is spherical and the size is small compared with the wavelength of excitation, the nanocrystal can be considered as a Rayleigh particle. Following our previous approach and ignoring the material birefringence [23], the electric field inside the nanocrystal can be found to be in-phase and uniform as $\mathbf{E}_P^{(\omega)} = \left[3\varepsilon_m / (\varepsilon_P + 2\varepsilon_m)\right]\mathbf{E}_m^{(\omega)}$ [37], where $\mathbf{E}_m^{(\omega)}$ is the incident electric field in the surrounding medium in the absence of the particle, and ε_P and ε_m are the linear permittivities of the particle and the surrounding medium respectively. The electric field $\mathbf{E}_P^{(\omega)}$ at the fundamental frequency ω is then decomposed into three orthogonal components along the three axes in the crystal frame, i.e. $\mathbf{E}_P^{(\omega)} = E_{CX}\hat{\mathbf{e}}_{CX} + E_{CY}\hat{\mathbf{e}}_{CY} + E_{CZ}\hat{\mathbf{e}}_{CZ}$, where $\hat{\mathbf{e}}_{CX}$, $\hat{\mathbf{e}}_{CY}$, and $\hat{\mathbf{e}}_{CZ}$ are unit vectors in the crystal frame as shown in Fig. 1 (a). The SHG polarizations along the three crystal axes are related to $\mathbf{E}_P^{(\omega)}$ by

$$\mathbf{P}^{(2\omega)} = \mathbf{d}\cdot\mathbf{E}_{\mathrm{P}}^{(\omega)}\cdot\mathbf{E}_{\mathrm{P}}^{(\omega)} = \begin{bmatrix} 0 & 0 & 0 & 0 & \mathrm{d}_{15} & 0 \\ 0 & 0 & 0 & \mathrm{d}_{15} & 0 & 0 \\ \mathrm{d}_{31} & \mathrm{d}_{31} & \mathrm{d}_{33} & 0 & 0 & 0 \end{bmatrix} \begin{bmatrix} \mathrm{E}_{CX}{}^2 \\ \mathrm{E}_{CY}{}^2 \\ \mathrm{E}_{CZ}{}^2 \\ 2\mathrm{E}_{CY}\mathrm{E}_{CZ} \\ 2\mathrm{E}_{CX}\mathrm{E}_{CZ} \\ 2\mathrm{E}_{CX}\mathrm{E}_{CY} \end{bmatrix}, \qquad (1)$$

where $\mathbf{d}$ is the second-order susceptibility tensor of the bulk $BaTiO_3$ crystal. The values we used in the simulation are $d_{15} = -41\times10^{-9}$ esu, $d_{31} = -43\times10^{-9}$ esu, and $d_{33} = -16\times10^{-9}$ esu [36].

Because of the subwavelength particle size, the electrostatic approximation holds, and the induced SHG polarizations are uniform inside the particle. By assuming also that the size of the particle is much smaller than the SHG wavelength, the SHG polarizations within the particle can be regarded as three orthogonal SHG dipoles with the amplitudes proportional to the strengths of the polarizations. These three orthogonal SHG dipole moments radiate like antennas at the SHG frequency. The total SHG radiation power W_0 can be found as [23]

$$\mathrm{W}_0 = \frac{\mathrm{c}\mathrm{k}^4\mathrm{V}^2}{12\pi\varepsilon_0}\left|\mathbf{P}^{(2\omega)}\right|^2, \qquad (2)$$

where c is the speed of light, k is the wave number at the SHG frequency, V is the volume of the nanocrystal, and ε_0 is the vacuum permittivity. Following Eqs. (1) and (2), one can find that the total SHG power radiated from these three orthogonal dipoles is dependent on the orientation of the nanocrystal and the excitation polarization. Without losing generality, we assume that the c-axis of the nanocrystal is oriented at ϕ_0 = 0 degrees in the following theoretical calculation. In Fig. 1(b), we calculate and plot the total SHG power radiated by these three orthogonal dipoles as a function of excitation polarization γ (with respect to the

#126083 - $15.00 USD Received 26 Mar 2010; revised 10 May 2010; accepted 13 May 2010; published 21 May 2010

X axis as shown in Fig. 1(a)) when the nanocrystal is orientated at θ_0 = 10, 50, and 90 degrees.

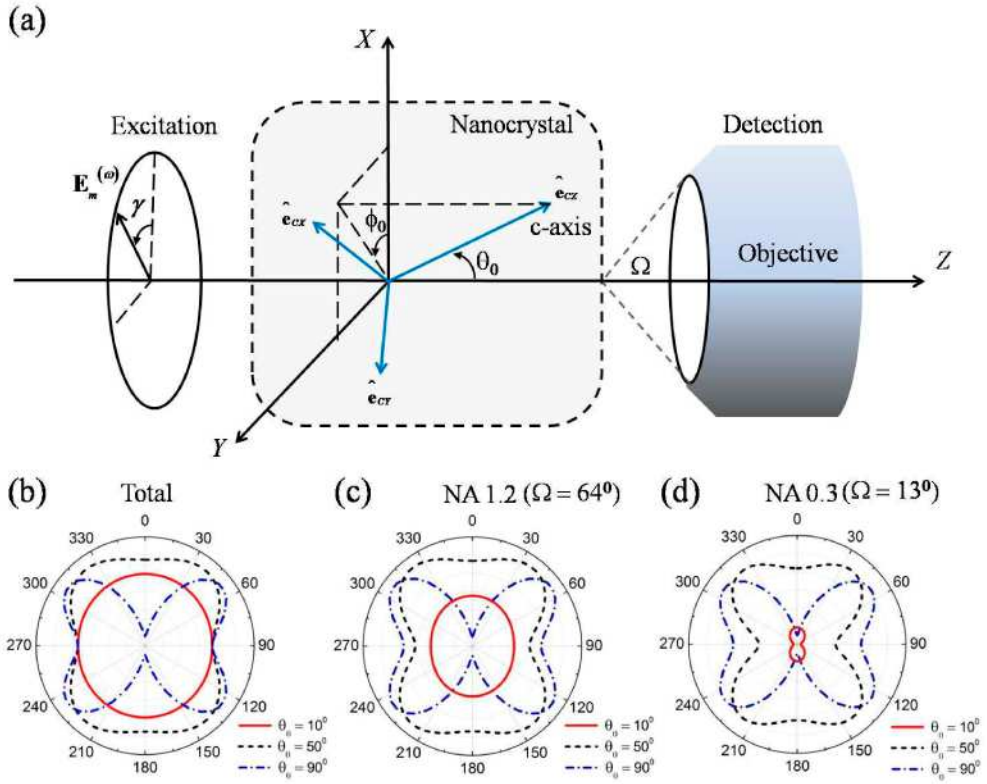

Fig. 1. Theoretical calculation of polarization dependent SHG response of a $BaTiO_3$ nanocrystal under a plane-wave excitation. (a) Schematic diagram of a $BaTiO_3$ nanocrystal oriented at an arbitrary direction under a LP excitation and the SHG signal is collected by a microscope objective. (b) The polarization dependency of the total SHG response of a $BaTiO_3$ nanocrystal. (c)(d) The polarization dependency of the SHG response of a $BaTiO_3$ nanocrystal where the SHG signal is collected by a (c) NA 1.2 water-immersion objective and (d) NA 0.3 water-immersion objective.

In nonlinear microscopy, the SHG signal is usually collected by a microscope objective. Since the SHG radiation is generally not a simple spherical wave, we further consider the collection efficiency provided by the objective to obtain an accurate estimation of the polarization dependent SHG response of a nanocrystal. The collection efficiency is determined by the overall far-field SHG intensity radiation pattern of the three orthogonal dipoles within the cone angle introduced by the objective. To calculate the collection efficiency, the three orthogonal dipoles are first projected back into the XYZ lab frame, namely $\mathbf{P}^{(2\omega)} = P_x\hat{\mathbf{e}}_X + P_y\hat{\mathbf{e}}_Y + P_Z\hat{\mathbf{e}}_Z$, where $\hat{\mathbf{e}}_X$, $\hat{\mathbf{e}}_Y$, and $\hat{\mathbf{e}}_Z$ are unit vectors in the lab frame. Each of the three new defined SHG dipoles radiates SHG field in the form of dipole radiation pattern [38]. Therefore, the SHG electric field radiation pattern in spherical coordinates can be related to $\mathbf{P}^{(2\omega)}$ as:

$$\mathbf{E}^{(2\omega)}(\mathbf{R}) \propto \begin{bmatrix} 0 & 0 & 0 \\ \cos\theta\cos\phi & \cos\theta\sin\phi & -\sin\phi \\ -\sin\phi & \cos\phi & 0 \end{bmatrix} \begin{bmatrix} P_x \\ P_y \\ P_z \end{bmatrix} \begin{matrix} \hat{\mathbf{e}}_R \\ \hat{\mathbf{e}}_\Theta \\ \hat{\mathbf{e}}_\Phi \end{matrix}, \qquad (3)$$

#126083 - $15.00 USD Received 26 Mar 2010; revised 10 May 2010; accepted 13 May 2010; published 21 May 2010

where $\hat{\mathbf{e}}_R$, $\hat{\mathbf{e}}_\Theta$, and $\hat{\mathbf{e}}_\Phi$ are the unit vectors in the spherical coordinate of the lab frame. The collection efficiency η can be easily found as the ratio of the SHG field intensity within the cone angle of the objective ($0 < \theta < \Omega$, $0 < \phi < 2\pi$) over the total SHG field intensity:

$$\eta = \frac{\int_0^{\Omega}\int_0^{2\pi}\left|\mathbf{E}^{(2\omega)}(\mathbf{R})\right|^2 \sin\theta\, d\phi\, d\theta}{\int_0^{\pi}\int_0^{2\pi}\left|\mathbf{E}^{(2\omega)}(\mathbf{R})\right|^2 \sin\theta\, d\phi\, d\theta}. \tag{4}$$

It is worth noting that η is a function of the cone angle Ω, the nanocrystal orientation, and the excitation polarization. We consider two cases where the SHG signal is collected by a high NA microscope objective (NA 1.2 water-immersion, Ω = 64.46 degrees) and a low NA microscope objective (NA 0.3 water-immersion, Ω = 13.04 degrees). Taking into account η for the collected SHG power, we plot the detected polarization dependent SHG responses for these two cases in Fig. 1(c) and (d) respectively. From Fig. 1(b), (c) and (d), it is obvious that higher NA detection gives a response closer to the total SHG signal. A substantial difference between Fig. 1(b)-(d) takes place when θ_0 is small. This is because a stronger axial dipole component (P_z) appears when θ_0 is small and the objective has a lower collection efficiency of the axial dipole than the transverse dipoles (P_x and P_y).

The orientation of a $BaTiO_3$ nanocrystal at the time of measurement under a LP plane-wave excitation can be assumed to be random and equally likely to be in any orientation in space. In a spherical coordinate system, the probability density function of a random orientation is a joint probability distribution of the angles θ and ϕ, which should lead to an equal probability of orientation within every unit solid angle. This requirement results in a probability density function of $f_{\Theta,\Phi}(\theta,\phi) = \sin\theta / 4\pi$. Note that the probability density function is not a uniform density function in the two angles θ and ϕ. With this assumption we can readily calculate the mean and the standard deviation of the measured SHG signal. The relative standard deviation (i.e. the standard deviation divided by the mean) of the measured SHG signal is calculated to be: 23.7% for the case of the total SHG signal detection, 28.5% for the case of NA 1.2 water-immersion objective detection, and 40.7% for the case of NA 0.3 water-immersion objective detection. The relative standard deviation of the signal increases significantly when the NA of the collection objective decreases. The effect of NA on the relative standard deviation of the SHG signal reflects the sensitivity of the collected SHG signal to the detection geometry, which is caused by the change in the SHG radiation pattern due to the combination of the nanocrystal orientation and the polarization dependent SHG response.

The relative standard deviation of the SHG signal under a LP excitation can be reduced if the excitation polarization can be rotated in the excitation plane (XY plane) within the time of measurement. When the excitation polarization rotates at an angular frequency much smaller than the optical frequency, it excites the nanocrystal in all polarization directions (still limited in the XY plane) and the polarization dependent SHG intensity due to the orientation variance in ϕ_0 is averaged out. We calculate the relative standard deviation of the measured SHG signal under this rotating LP plane-wave excitation. We found the relative standard deviation is reduced to: 9.5% for total SHG signal detection, 11.9% for NA 1.2 water-immersion objective detection, and 22.6% for NA 0.3 water-immersion objective detection.

We further calculate the SHG response under a CP excitation. A CP excitation can be resolved into two perpendicular LP excitations, of equal amplitude, and in phase quadrature. Therefore, we can calculate the SHG response of a nanocrystal under a CP excitation based on the model established above for the LP excitation. The SHG response is plotted as a function of the nanocrystal orientation in Fig. 2. Due to the symmetry of the crystal structure,

#126083 - $15.00 USD Received 26 Mar 2010; revised 10 May 2010; accepted 13 May 2010; published 21 May 2010

the SHG response from a $BaTiO_3$ nanocrystal is not sensitive to the handedness of CP excitations. In Fig. 2, we find that SHG signal monotonically decreases to zero when θ_0 decreases from 90 degrees to 0 degrees. This is the result of the interference effect between the two perpendicular LP excitations in quadrature resolved from the CP excitation and also the change of the effective nonlinear tensor due to the crystal orientations. Since the total SHG signal from the nanocrystal oriented at small θ_0 under a LP excitation is considerable as shown in Fig. 1(b), the vanishing SHG signal of the nanocrystal oriented at small θ_0 under a CP excitation is therefore mostly due to the interference effect.

The relative standard deviation of the measured SHG signal under a CP plane-wave excitation is found to be 38 ± 3% for the cases ranging from the total SHG signal detection to low NA detection (NA 0.3 water-immersion objective). It is worth noting that the relative standard deviation of the SHG signal under CP excitation is much greater than that under the rotating LP excitation described previously. The increase in the relative standard deviation shows that the nanocrystal has different SHG response under a rotating LP excitation and a CP excitation. It is also interesting to notice the small variation (±3 %) in the relative standard deviation when the NA of the collection objective changes. This implies that, under a CP excitation, the SHG radiation pattern does not vary a lot as the nanocrystal orientation changes. In fact, the radiation pattern is always dominated by the transverse dipoles (P_x and P_y), which is less sensitive to the NA of detection.

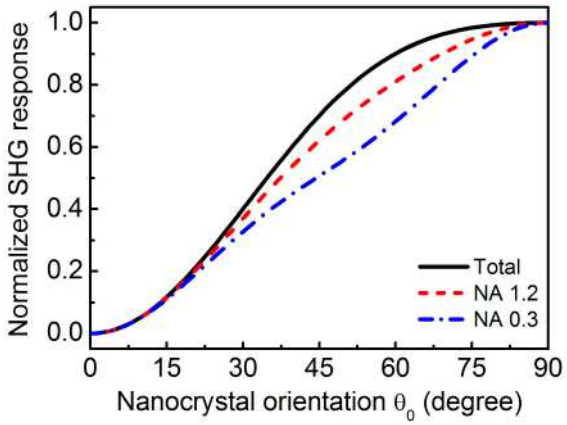

Fig. 2. Theoretical calculation of the normalized SHG response of a $BaTiO_3$ nanocrystal as a function of nanocrystal orientation under a CP plane-wave excitation. Different detection schemes are considered: total SHG response (black solid curve), collected by an NA 1.2 water-immersion objective (red dash curve), and collected by an NA 0.3 water-immersion objective (blue dash-dot curve).

2.2 SHG from nanocrystals under a tightly focused excitation

In nonlinear scanning microscopy, the excitation is tightly focused and scanned across the sample to form an image. The depolarization of the LP excitation being tightly focused by a high NA objective has been studied [33]. The depolarization effect gives rise to new excitation polarizations at the focus which then participate in the SHG. As a result, the depolarization may change the SHG polarization response significantly due to the nature of SHG (as described in Eq. (1)). We simulate the SHG response of a nanocrystal in a scenario of a scanning microscope. It is convenient to introduce spherical polar coordinates as shown in Fig. 3(a). A LP (X -polarized) plane-wave excitation propagating in the Z direction of 812 nm wavelength is tightly focused by a NA 1.2 water-immersion objective and the beam waist is at $Z = 0$. The focused field at the beam waist can be written as [33]:

#126083 - $15.00 USD Received 26 Mar 2010; revised 10 May 2010; accepted 13 May 2010; published 21 May 2010

$$
\begin{aligned}
E_X(r,\phi) &= -i\left[f_0(r) + f_2(r)\cos(2\phi)\right] \\
E_Y(r,\phi) &= -i\, f_2(r)\sin(2\phi) \\
E_Z(r,\phi) &= -2 f_1(r)\sin(\phi)
\end{aligned}
\quad , \tag{5}
$$

where

$$
\begin{aligned}
f_0(r) &= \int_0^{\Omega} \sqrt{\cos\theta}\,\sin\theta(1+\cos\theta) J_0(kr\sin\theta)\, d\theta \\
f_1(r) &= \int_0^{\Omega} \sqrt{\cos\theta}\,\sin^2\theta J_1(kr\sin\theta)\, d\theta \\
f_2(r) &= \int_0^{\Omega} \sqrt{\cos\theta}\,\sin\theta(1-\cos\theta) J_2(kr\sin\theta)\, d\theta
\end{aligned}
\quad , \tag{6}
$$

and $r = \sqrt{X^2 + Y^2} > 0$, $0 \le \phi < 2\pi$. $J_n(\cdot)$ is the Bessel function of the first kind and order n.

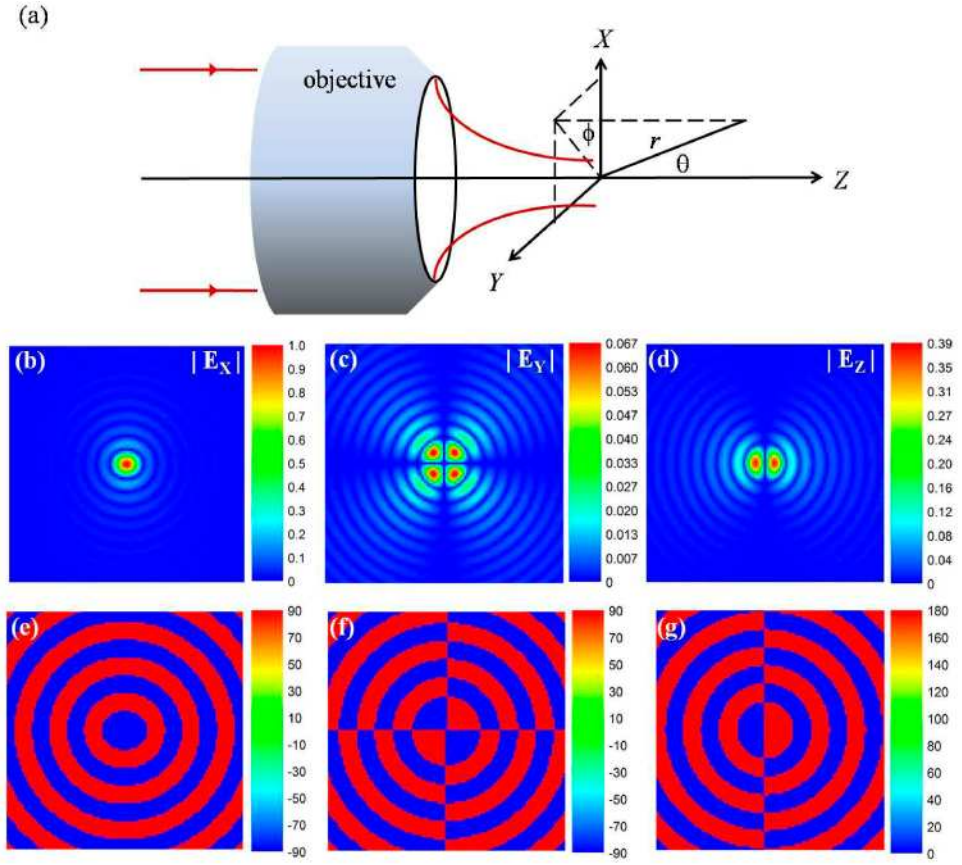

Fig. 3. Theoretical calculation of the tightly focused LP (X-polarized) excitation. (a) Schematic diagram of a tightly focused excitation by using a microscopic objective. The magnitude (b)-(d) and the phase (e)-(g) of the electric field of X-, Y-, Z-polarizations at the focused beam waist (Z = 0). The incidence is an X-polarized plane-wave of 812 nm wavelength which is focused by a NA 1.2 water-immersion objective in an index-matching environment. The size of the images are $6 \times 6\ \mu m^2$.

The magnitudes and the phases of the three perpendicularly polarized fields at the beam waist $E_i\big|_{Z=0}$, $i = X, Y, Z$, are plotted in Fig. 3(b)-(d) and (e)-(g) respectively. Besides the field

#126083 - $15.00 USD Received 26 Mar 2010; revised 10 May 2010; accepted 13 May 2010; published 21 May 2010

at the original polarization (i.e. $|E_X|_{Z=0}$), a considerable amount of axial component $|E_Z|_{Z=0}$ appears which will participate in the SHG process.

In a scanning microscope, the calculated complex excitation patterns described in Eq. (5) are scanned across a nanocrystal and a scanning image of a nanocrystal is formed. The pixel size in Fig. 3(b)-(d) is 60 ´ 60 nm^2, corresponding to a scanning step size of 60 nm. Assuming the nanocrystal is much smaller than the focused spot of the excitation, while the excitation patterns is scanned across, it will pick up the local excitation fields calculated at each pixel as a plane-wave excitation and emit SHG signal as described in the previous section. Under this assumption, the theoretical SHG scanning image can be obtained by calculating the SHG signal from the nanocrystal pixel-by-pixel based on the excitation patterns. The finite size of the nanocrystal in reality would make the measured SHG response deviate from this theoretical estimation. More discussions on the validity of this assumption can be found in the Discussion Section. We integrate the SHG intensity over the whole scanning image to represent the SHG response of a nanocrystal at certain orientation and under a specific excitation polarization using a scanning microscope.

The theoretical polarization dependent SHG response of a nanocrystal under a tightly focused excitation (NA 1.2 water-immersion objective) is plotted in Fig. 4 where the nanocrystals orientated at θ_0 = 10, 50, and 90 degrees are considered. Similar to the analysis of plane-wave excitation, we calculate the total SHG signal and also the signal collected by NA 1.2 and NA 0.3 water-immersion objectives, as shown in Fig. 4(a), (b), and (c) respectively. We find Fig. 4(a)-(c) have a similar behavior as Fig. 1(b)-(d), i.e. the decrease of the collected SHG signal when the NA decreases at small θ_0, which is due to the collection efficiency of the objective. We also find that a tightly focused beam results in a slightly different SHG polar response from a uniform excitation: where the uniform excitation gives a weak SHG signal, such as θ_0 = 90 degrees and γ = 0 degrees, the tightly focused excitation gives a stronger SHG signal due to the depolarization effect. In other words, the depolarization effect induces new excitation polarizations, which results in an averaging effect in the SHG polar response.

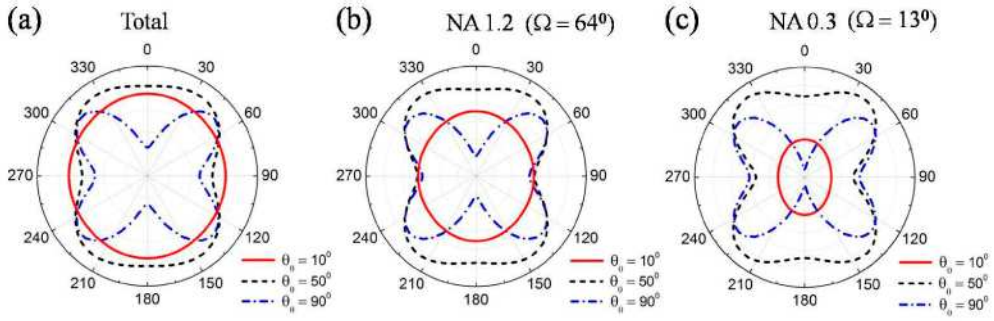

Fig. 4. Theoretical calculation of the polarization dependent SHG response of a $BaTiO_3$ nanocrystal in a scanning image with a tightly focused excitation (NA 1.2 water-immersion objective). (a) The polarization dependency of the total SHG response of a $BaTiO_3$ nanocrystal. (b)(c) The polarization dependency of the SHG response of a $BaTiO_3$ nanocrystal where the SHG signal is collected by a (b) NA 1.2 water-immersion objective and (c) NA 0.3 water-immersion objective.

To evaluate the averaging effect due to the tightly focused excitation, we calculate the relative standard deviation of the SHG signal as described previously. The relative standard deviation is calculated to be: 19.6% for the case of the total SHG signal detection, 23.6% for the case of NA 1.2 water-immersion objective detection, and 33.5% for the case of NA 0.3

#126083 - $15.00 USD Received 26 Mar 2010; revised 10 May 2010; accepted 13 May 2010; published 21 May 2010

water-immersion objective detection. The smaller relative standard deviation shows that a tightly focused excitation can reduce the variance of the polarization dependent SHG signal.

We calculate the relative standard deviation of the SHG signal with rotating LP excitation when it is tightly focused. The relative standard deviation is: 11.0% for total SHG signal detection, 11.7% for NA 1.2 water-immersion objective detection, and 17.3% for NA 0.3 water-immersion objective detection. The averaging effect due to the rotating LP excitation is again obvious.

We further calculate the SHG response of a nanocrystal under a tightly focused CP excitation. Analogous to the plane-wave excitation, the CP excitation is first resolved into two perpendicular LP excitations of equal amplitude and in phase quadrature, and then depolarized through tightly focusing respectively. The excitation field patterns of a tightly focused CP can be found, and therefore the SHG response can be calculated. The normalized SHG response is plotted as a function of the nanocrystal orientation in Fig. 5, which is significantly different from Fig. 2. While the normalized SHG response drops from 0.3 to 0 as θ_0 decreases from 30 degrees to 0 degrees for the plane-wave excitation (in Fig. 2), it remains at around 0.3 for the tightly focused excitation (in Fig. 5). This is because the SHG polarization induced by the tightly focused CP excitation does not cancel out completely due to the depolarization effect.

We also calculate the relative standard deviation of the SHG signal under a tightly focused CP excitation. The relative standard deviation is calculated as ~27±1% for the cases ranging from the total SHG signal detection to low NA detection (NA 0.3 water-immersion objective). The much smaller relative standard deviation compared with the CP plane-wave excitation (38 ± 3%) again shows that a tightly focused excitation can reduce the variance of the polarization dependent SHG signal. The small range (±1%) of the relative standard deviation is also consistent to the case of CP plane-wave excitation.

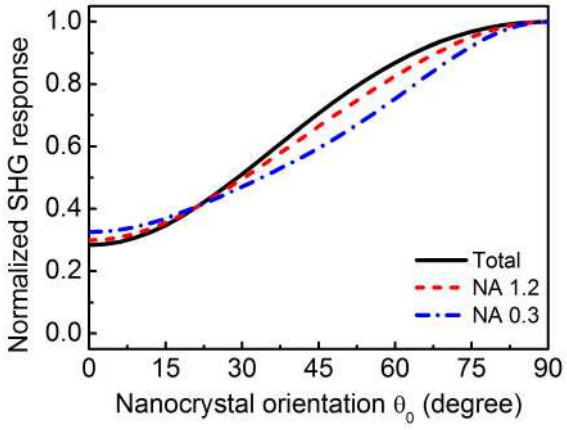

Fig. 5. Theoretical calculation of the normalized SHG response of a $BaTiO_3$ nanocrystal as a function of nanocrystal orientation under a CP tightly focused excitation. Different detection schemes are considered: total SHG response (black solid curve), collected by an NA 1.2 water-immersion objective (red dash curve), and collected by an NA 0.3 water-immersion objective (blue dash-dot curve).

We summarize the relative standard deviation of the SHG signal from a $BaTiO_3$ nanocrystal under different excitation geometry (plane-wave and tightly focused excitations) of different polarizations (LP, rotating LP and CP) and also for different NA of the detection in Table 1. It is clear to see that the focused excitation and the high NA of the detection can reduce the effect of polarization dependent SHG signal. The difference between the rotating LP excitation and CP excitation is obvious. In the case of CP excitation, both for the plane-wave and focused excitations, the relative standard deviation of the SHG signal is not

#126083 - $15.00 USD Received 26 Mar 2010; revised 10 May 2010; accepted 13 May 2010; published 21 May 2010

sensitive to the NA of detection. However, the relative standard deviation of the SHG signal is usually greater under CP excitation than under LP excitation. The CP excitation only provides lower relative standard deviation in the signal when the NA of detection is low.

Table 1. Relative standard deviation of the SHG signal

		Total	NA 1.2 detection	NA 0.3 detection
Plane-wave excitation	LP	23.7%	28.5%	40.7%
	Rotating LP	9.5%	11.9%	22.6%
	CP	35.6%	37.2%	41.0%
Focused excitation (NA 1.2)	LP	19.6%	23.6%	33.5%
	Rotating LP	11.0%	11.7%	17.3%
	CP	25.9%	26.4%	27.8%

3. Experimental results

We used a standard scanning confocal microscope (Leica SP5) to excite and to detect SHG signal from individual $BaTiO_3$ nanocrystals. The X-ray diffraction pattern (data not shown) confirms the crystal structure is tetragonal which is non-centrosymmetric and allows for efficient SHG without further treatment. Isolated nanocrystals were deposited on an indium-tin-oxide (ITO) coated glass slide and then immersed in water for the confocal microscope measurement with a water-immersion objective. Figure 6 is a typical scanning electron microscope (SEM) image of the nanocrystals prepared on an ITO coated glass slide. It shows that the nanocrystals are nearly spherical in shape and around 90 nm in diameter. It also shows that most of the nanocrystals on the glass slide are isolated single nanocrystals. The excitation light source was a Ti:Sapphire oscillator (Chameleon Ultra II, Coherent) generating 140 fs laser pulses at 812 nm wavelength and 80 MHz repetition rate. The average excitation power is approximately 15 mW. The excitation was tightly focused by a 63x NA 1.2 water-immersion objective and the SHG signal was collected by the same objective in an epi-geometry. The SHG signal was detected by a photomultiplier (R6357, Hamamatsu) and the ambient light was rejected by a narrow bandpass optical filter centered at 406 nm with 15 nm bandwidth. The excitation polarization is controlled by a half-wave plate or a quarter-wave plate placed in the excitation beam before it enters the confocal microscope.

Figure 7 shows a typical SHG confocal image of the nanocrystals under a LP excitation, where the sample was prepared in a similar way as for the SEM measurement. The SHG signal from individual nanocrystals shows great contrast. The background SHG from the ITO/water interface is relatively weak. The pixel size in Fig. 7 is 60 ´ 60 nm^2. The full width at half maximum (FWHM) of the SHG imaging spot size of the $BaTiO_3$ nanocrystal is about 300 nm, which matches well with the diffraction limited spot size at the SHG wavelength based on a tightly focused excitation beam described in the previous section. The SHG intensity of individual nanocrystals varies due to the size-dependent and also the polarization-dependent SHG signal. Based on the SHG efficiency of $BaTiO_3$ nanocrystals described in Ref. 23, we estimate the average power of the SHG signal from the $BaTiO_3$ nanocrystals in our measurement is approximately 10 −100 pW.

#126083 - $15.00 USD Received 26 Mar 2010; revised 10 May 2010; accepted 13 May 2010; published 21 May 2010

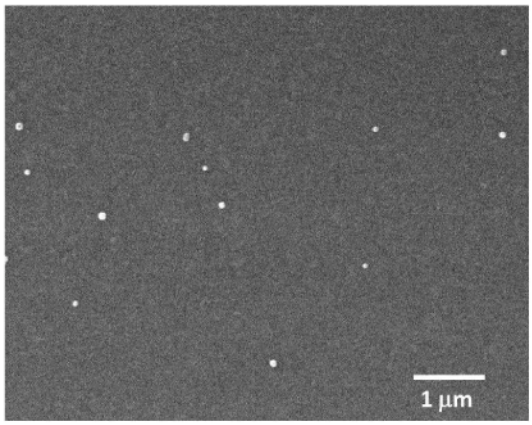

Fig. 6. SEM image of isolated $BaTiO_3$ nanocrystals randomly deposited on an ITO coated glass substrate for SHG polarization measurement. Most of the nanocrystals are 60-110 nm in diameter.

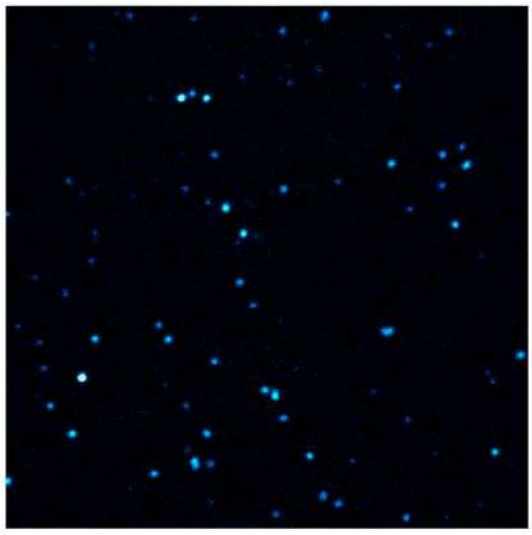

Fig. 7. Scanning confocal SHG image of $BaTiO_3$ nanocrystals on an ITO coated glass substrate. The size of the image is 30 ´ 30 μm^2.

We measured the polarization dependent SHG response from individual nanocrystals by rotating LP excitation with a half-wave plate. One SHG confocal image was captured for each excitation polarization direction. The excitation polarization was rotated from 0 to 180 degrees with a 10-degree angular step size. We calibrated the excitation power at the sample position as it varies about 5% when the excitation polarization changes due to the polarization dependent response of the confocal microscope. The SHG response of individual nanocrystals was found by integrating the SHG signal within the bright spot in the confocal image, while the background SHG from the ITO/water interface was subtracted. We measured the polarization dependent SHG response of 39 nanocrystals. Figure 8 shows two representative polar diagrams of the SHG response of $BaTiO_3$ nanocrystal as a function of the excitation polarization. From the measured responses, we can find the orientations of the nanocrystals by fitting with theoretical calculation (corresponding to the results shown in Fig. 4 (b)). The fitting of the orientation of the nanocrystal is unique because each (θ_0 , ϕ_0) pair gives a different polar response except the ambiguity between ϕ_0 and $\phi_0 + 180$ degrees. The measured

#126083 - $15.00 USD Received 26 Mar 2010; revised 10 May 2010; accepted 13 May 2010; published 21 May 2010

responses agree well with the theoretical calculation. In Fig. 8, the two nanocrystals were found oriented at $\theta_0 = 70 \pm 5$ degrees, $\phi_0 = 35 \pm 5$ degrees and at $\theta_0 = 50 \pm 5$ degrees, $\phi_0 = 115 \pm 5$ degrees respectively. The 10 degrees resolution of the fitting is due to the accuracy of the measurement. We did the fitting to all 39 nanocrystals, and various orientations of the nanocrystals (θ_0 from 30 to 80 degrees) were observed from the measurement.

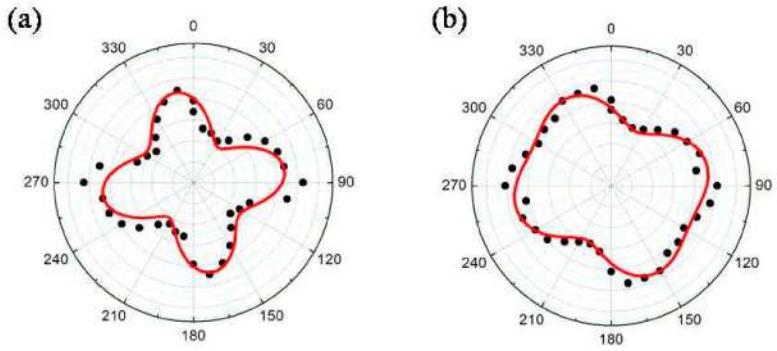

Fig. 8. (a) (b) Polarization dependent SHG response of two representative $BaTiO_3$ nanocrystals measured by a scanning confocal microscope. The experimental data are shown as black dots and the theoretical fits are shown as red lines.

We further measured the SHG response of the same 39 nanocrystals under a CP excitation by replacing the half-wave plate with a quarter-wave plate at a proper orientation. The CP excitation intensity was kept the same as the LP excitation on the sample position. All the nanocrystals were observed under a CP excitation. Following the identical image processes, we found the SHG response of the nanocrystals under a CP excitation.

We compared the measured SHG response of a nanocrystal under a CP excitation with that under LP excitations of the same intensity. Since the SHG response depends on the excitation polarization γ under LP excitation, we use the average SHG response over the angle of excitation polarization γ from 0 to 2π for the comparison. Specifically, we define $\rho_{CP/LP}$ as the ratio of the SHG response under a CP excitation to the average SHG response under LP excitations of the same excitation intensity:

$$\rho_{CP/LP}(\theta_0) = \frac{W_{CP}(\theta_0)}{\int_0^{2\pi} W_{LP}(\theta_0,\gamma)\,d\gamma \Big/ 2\pi}, \tag{7}$$

where $W_{CP}(\theta_0)$ is the SHG power from a nanocrystal oriented at θ_0 under a CP excitation, and $W_{LP}(\theta_0,\gamma)$ is the SHG power from a nanocrystal oriented at θ_0 under a LP excitation at excitation polarization angle γ.

From the measured SHG responses of the nanocrystals under CP and LP excitations, we obtained the ratio $\rho_{CP/LP}$ for each of the measured 39 nanocrystals. The values of the ratio $\rho_{CP/LP}$ are plotted with the corresponding fitted nanocrystal orientations θ_0 for all 39 nanocrystals in Fig. 9. We also plot the theoretical calculation of $\rho_{CP/LP}$ in Fig. 9, which is based on the model described in Section 2.2, considering the tightly focused excitation and the collection efficiency provided by the objective. We found the experimental data agrees with the theoretical calculation. In Fig. 9, it is clear that the SHG response of a nanocrystal

#126083 - $15.00 USD Received 26 Mar 2010; revised 10 May 2010; accepted 13 May 2010; published 21 May 2010

under CP excitation is not simply an average of the SHG responses under LP excitations over the excitation polarizations (otherwise the curve should be a flat line at value of 1).

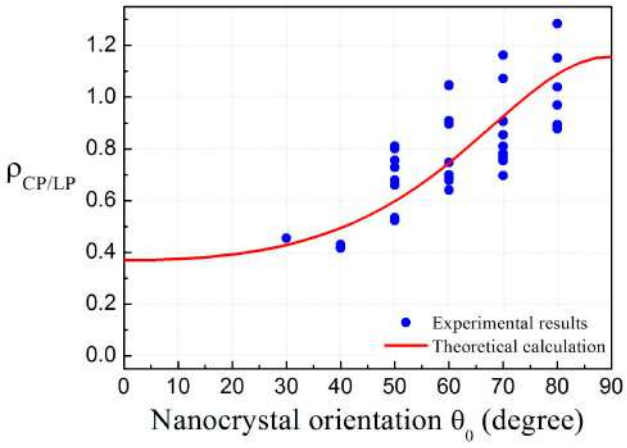

Fig. 9. Relative SHG response of 39 $BaTiO_3$ nanocrystals under CP and LP tightly focused excitations correlated to the nanocrystal orientations. The red solid curve is the theoretical calculation considering a tightly focused excitation, while the blue dots are the experimental results.

4. Discussion

In the theoretical calculation, we assume the size of the nanocrystal is much smaller than the focused spot. In the experiment, the size of the nanocrystals was around 90 nm in diameter. In comparison, the tightly focused spot size using an NA 1.2 water-immersion objective at 812 nm wavelength is about 480 nm FWHM transversely, which is more than 5 times greater than the particle size. In the axial direction, the depth of focus of the excitation is about 1 μm FWHM which is more than 10 times greater than the particle size. These dimensions support our assumption of the electrostatic approximation. The good match between the measured and calculated polarization dependent SHG responses shows the theoretical calculation is able to provide reasonable estimation. It also suggests our simple theoretical model in which the local excitation field of the nanocrystal is assumed to be a plane-wave, is valid in our experiment. Furthermore, it has been reported that for the particle size smaller than 150-200 nm in diameter under a tightly focused excitation at 945 nm wavelength, it is reasonable to use the single dipole approximation for the SHG emission [18]. Therefore, we believe the single dipole approximation is also valid for 90 nm diameter particle under the 812 nm wavelength excitation as in our scenario. In cases where we need to find a more accurate solution (i.e. for larger particles), one would need to calculate the excitation field inside the nanocrystal under a tightly focused excitation.

It is interesting to consider the SHG response due to the abrupt 180 degrees phase change in the tightly focused excitation pattern at the beam waist as shown in Fig. 3 (e)-(g). During the scanning, when the nanocrystal is at the boundary of the abrupt phase change, we will have an out-of-phase excitation on its two sides. The plane-wave excitation approximation will not hold in this situation. However, the magnitude of the excitation field is always weak at these boundaries of abrupt phase change. Therefore, the abrupt phase change in the excitation pattern should have little effect on the overall SHG response. Furthermore, the Gouy phase shift of the focusing in the axial direction should also have little effect on the SHG response because the nanocrystal is small compared with the depth of focus of the excitation.

We note that it has been reported an extra ellipticity in the excitation polarization may be introduced from the scanning system and the dichroic mirror due to their polarization

#126083 - $15.00 USD Received 26 Mar 2010; revised 10 May 2010; accepted 13 May 2010; published 21 May 2010

sensitive reflective properties [9,39,40]. However we have not observed a substantial ellipticity polarization introduced to the excitation in our imaging system. The degree of polarization (DOP) is measured to be between 0.92 and 0.98 for all the LP excitations. The theoretical calculation shown in Fig. 9 is under the assumption that DOP is equal to 1. We roughly estimate the overall ellipticity effect in our system with the averaged value of DOP as 0.95 by using a corresponding elliptical polarization as the excitation in the calculation. By taking into account the ellipticity in the excitation, we plot the theoretical ratio $\rho_{CP/LP}$ as a function of nanocrystal orientation θ_0 in Fig. 10, along with the experimental data. The two theoretical calculations for DOP as 0.95 and 1 show similar behaviors, and they reasonably agree with the experimental data. Slightly more derivation is observed at small θ_0 which may be due to the imperfect measurement. Therefore, we believe the ellipticity effect in the excitation polarization in our system is not significant.

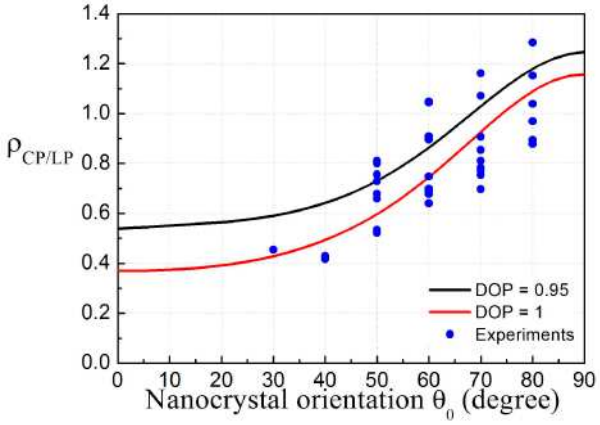

Fig. 10. Evaluation of the ellipticity effect in the excitation polarization on the relative SHG response of $BaTiO_3$ nanocrystals under CP and LP tightly focused excitations correlated to the nanocrystal orientations. The black/red curves are the theoretical calculations considering with/without ellipticity in the excitation introduced by the system, while the blue dots are the experimental results.

5. Conclusion

We studied the SHG response from $BaTiO_3$ nanocrystals under various excitations. Theoretical models were developed to describe the SHG from nanocrystals under both plane-wave and tightly focused excitations. Based on our studies, we found the depolarization effect of the excitation caused by the high NA objective can have substantial effect on the SHG signal. We studied the effect of NA of the microscope objective in the SHG signal collection. Low NA detection is sensitive to the SHG radiation pattern of the nanocrystal and therefore the polar response can be very different from the total SHG signal. We also compared the SHG signal under CP and LP excitations. While the CP excitation can be used as an alternative choice of excitation for SHG microscopy, we show that the SHG response under CP excitation is generally inferior to the average of LP excitations over all orientations. To verify our theoretical models, we measured the polarization dependent SHG responses from $BaTiO_3$ nanocrystals with a scanning confocal microscope. A good agreement between the theoretical calculation and experimental data was observed. The complete knowledge of the polarization dependence of the SHG response from nanocrystals will be necessary in applications where SHRIMPs are used as imaging probes for position and rotation detection.

#126083 - $15.00 USD Received 26 Mar 2010; revised 10 May 2010; accepted 13 May 2010; published 21 May 2010

Acknowledgements

The authors thank Dr. Paul Bowen at EPFL for providing the $BaTiO_3$ nanocrystals. This project is supported by the National Center of Competence in Research (NCCR), Quantum Photonics.

#126083 - $15.00 USD Received 26 Mar 2010; revised 10 May 2010; accepted 13 May 2010; published 21 May 2010